Astronomical and Astrophysical Transactions (*AApTr*), 2025, Vol. 35, Issue 4, pp. 449–456,
ISSN 1055-6796, Photocopying permitted by license only, ©Cambridge Scientific Publishers

Water in L1544: 2-phase and 3-phase approaches

O.V. Kochina[1,*], D.S. Wiebe[1], M.S. Kirsanova[1,2]

[1] *Institute of Astronomy, Russian Academy of Sciences, 119017, 48 Pyatnitskaya Str., Moscow, Russia*
[2] *Lebedev Physical Institute, Russian Academy of Sciences, Moscow, Russia*

Received 18 June, 2025; accepted 17 August, 2025

Water is a vital but poorly constrained component in star-forming regions, with its interstellar origins holding implications for planetary system formation and the delivery of water to terrestrial planets. The prestellar core L1544, a potential precursor to the early Solar System, offers a unique opportunity to study water chemistry in a cold collapsing environment. Using the 1D chemical code Presta, we model the evolution of water in L1544, comparing traditional two-phase (gas + ice) and advanced three-phase (gas + surface ice + bulk ice) approaches. The model incorporates observationally constrained density/temperature profiles and contains a comprehensive chemical network. The three-phase approach allows tracking water partitioning between surface and bulk ice reservoirs. Analysis of the reaction rates confirms that gas-phase water primarily originates from grain-surface chemistry. The dominant formation pathway is through the surface reaction s-H + s-OH $\longrightarrow$ s-H_2O. Immediately upon the formation, the majority ($\sim$95%) of water molecules undergo rapid sequestration into the bulk ice phase. The remaining fraction is subject to reactive desorption, a non-thermal process whereby the energy released during surface reactions (in this case, water formation) ejects a part of the products (5%) into the gas phase. This mechanism serves as the primary channel for replenishing gas-phase water in cold, dense environments, maintaining the observed balance between ice mantle growth and molecular gas abundances.

Keywords: Water, star formation, ISM, astrochemistry

1 Introduction

Water, a critical component for terrestrial life, covers $\sim$70% of Earth's surface and also presents in the atmosphere in highly variable amounts. Despite its apparent abundance, water constitutes only a minor fraction of Earth's total mass. Its origin remains uncertain: it may have been present during Earth's formation 4.6 Gyr ago or delivered later via impacts of asteroids, comets, or meteorites – remnants of the protoplanetary disk. Leading models suggest that the inner Solar System was initially hot

*Email: okochina@inasan.ru

and dry, so water had arrived from the outside during the Late Heavy Bombardment or similar accretion events (Izidoro & Piani 2022, Kirsanova et al. 2025).

The detection of interstellar water in star-forming molecular clouds in the late 1960s (Snyder & Buhl 1969, Cheung et al. 1969) initiated systematic studies of its distribution across cosmic environments. However, atmospheric water vapor severely hampers ground-based observations, necessitating the use of high-altitude facilities, airborne telescopes, and space observatories. Early space missions like ESA's ISO or NASA's Spitzer provided initial constraints, but were unable to observe fundamental ground-state water transitions in the far-infrared/submillimeter regime, leaving cold prestellar cores largely unexplored. The Herschel Space Observatory overcame these limitations with its HIFI instrument, which achieved unprecedented spectral resolution and detected approximately 40 rotational water transitions. The main results of the WISH Key Program (Water in Star-forming Regions with Herschel) are summarized by van Dishoeck et al. (2021).

The WISH Key Program made the first detection of water vapor in a cold dense prestellar core Lynds 1544 (L1544 below) in the Taurus molecular cloud (Caselli et al. 2012). Herschel's observations revealed water vapor equivalent to >2000 Earth oceans, sublimated from icy dust grains, with an additional thousand times more water locked in ice. This reservoir suggests that future planets forming in this object may inherit this water content.

The core contains sufficient mass to form a solar-mass star, suggesting the potential for a planetary system with characteristics similar to our own. Studies of L1544 hold particular significance as it may represent a direct analog to a precursor of the Solar System. This unique window into early star and planet formation processes could provide crucial insights into the origins of our own planetary system, water and life on Earth.

The aim of the present study is to model evolution of water abundance in L1544, comparing traditional two-phase (gas + ice) model used by Caselli et al. (2012) and advanced three-phase (gas + surface ice + bulk ice) approaches. We describe the observed properties of L1544 in Sec. 2. The model we use is described in Sec. 3. Comparison of the two-phase and three-phase models is presented in Sec. 4.

2 L1544

L1544 is a well-studied prestellar core embedded in the Taurus molecular cloud complex, situated at a distance of 170 parsecs (Galli et al. 2019). This core exhibits a quiescent dynamical environment, characterized by a high central density and low central temperature. Observations reveal pronounced infall kinematics, indicative of ongoing gravitational collapse in the early stages of star formation.

The study by Caselli et al. (2012) presents the first detection of water vapor in the pre-stellar core L1544 using the Herschel Space Observatory. Observations were targeted to the ground-state transition of ortho-H_2O (1_{10}–1_{01}) at 557 GHz. The detected water line exhibits an inverse P-Cygni profile, a signature of gravitational contraction, with blue-shifted emission and red-shifted absorption. This profile indicates that water vapor is present in the cold, dense central region of L1544 (within a few thousand AU), where heavy molecules like water are typically expected to freeze

onto dust grains. The study estimates the water vapor abundance in the core center to be at least 10^{-9} relative to H_2, corresponding to a total mass of $\sim 1.5 \times 10^{-6}\, M_\odot$.

To interpret the observations, the authors combined radiative transfer modeling with chemical and dynamical simulations. The models account for the effects of cosmic-ray-induced desorption, freeze-out, and gas-grain chemistry, revealing that the detected water vapor is sustained by a balance between freeze-out and photodesorption. The model outputs, presented in Caselli et al. (2012, their Fig. 3), serve as the reference framework for our comparative analysis of chemical modeling results.

3 Modelling

The chemical modeling of L1544 was performed using Presta, a one-dimensional code for simulating the chemical evolution of spherically symmetric clouds under both external diffuse UV radiation and central protostellar irradiation (Kochina et al. 2013). The model divides the object into concentric cells with individually specified density, gas temperature, and dust temperature profiles based on Caselli et al. (2012), assuming no mass exchange between cells. The UV radiation intensity is calculated from dimensionless values at the domain boundaries and the visual extinction A_V for each cell. Presta operates in a quasi-time-dependent mode with static physical conditions manually assigned according to observed profiles. We deliberately initiate our study of L1544 with a static model to examine molecular distribution patterns in both two- and three-phase models.

The model consists of a spherically symmetric core with a radius of 0.2 pc, exhibiting strong density fall-off from 4×10^6 cm^{-3} in the core center to 6×10^2 cm^{-3} at the outer edge. The temperature profile shows more moderate variation, ranging from 6 K in the center to 11 K at the periphery (see Fig. 1 for detailed profiles).

The code incorporates comprehensive chemical processes, including gas-phase reactions (cosmic ray interactions, two-body processes, photoreactions (including cosmic ray-induced photons) and dissociative recombination), as well as grain-surface chemistry (adsorption, desorption, and reactive processes). Since the three-phase approach has been implemented in previous studies by other authors (see, e.g., Ruaud & Gorti 2019 for protoplanetary disks; Maitrey et al. 2025 for cold cores) with results showing good agreement with observations, we also adopt a three-phase treatment in this study. The implemented approach (Borshcheva & Wiebe 2022) accounts for both surface reactions and mantle bulk reactions. The phase transfer mechanism follows the formulation described in Hasegawa & Herbst (1993). This study presents a comparison between the traditional two-phase and the advanced three-phase approaches, implementing reactive desorption with a fixed 5% product release efficiency.

Kinetic equations are integrated individually for each cell using the ALCHEMIC chemical network (Semenov and Wiebe 2011) with updates from Wiebe et al. (2019). Presta includes a reaction pathway analyzer that identifies dominant formation and destruction mechanisms for selected species. The model outputs include both radial abundance profiles and central column densities at specified evolutionary times, providing a complete chemical characterization of the prestellar core.

We employ the low-metal elemental abundances from Lee et al. (1996), where heavy elements are predominantly locked in dust grains and thus excluded from the

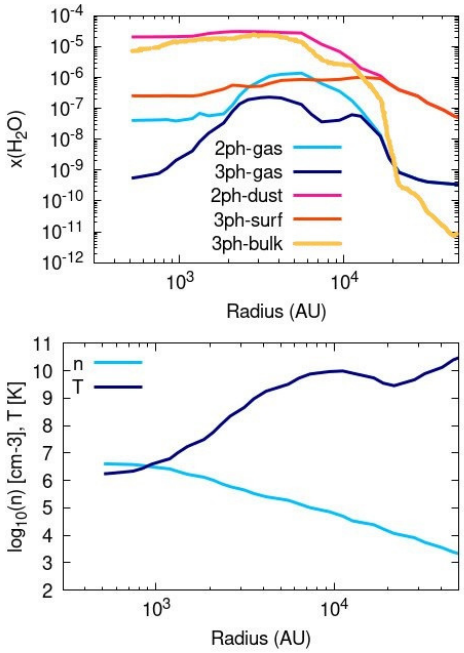


Figure 1 Chemical modeling results for L1544. Bottom panel: Radial profiles of physical parameters – gas temperature (dark blue curve) and H_2 number density (light blue curve). Top panel: Water abundance distributions showing: gas-phase water in two-phase (light blue) and three-phase (dark blue) models; grain-surface water in two-phase approach (pink); and three-phase water components – surface (orange) and bulk ice (yellow). All abundances are relative to total hydrogen density.

Table 1 Initial component abundances used by PRESTALINE, relative to hydrogen.

Component	Abundance
C	7.3×10^{-5}
N	2.1×10^{-5}
O	1.7×10^{-4}
F	2.0×10^{-8}
He	1.4
Si+	3.0×10^{-9}
S+	2.0×10^{-8}
Cl+	3.0×10^{-9}
Na+	3.0×10^{-9}
Mg+	3.0×10^{-9}
Fe+	3.0×10^{-9}
P+	3.0×10^{-9}
Dust	2.0×10^{-11}

gas-phase chemistry. The complete set of adopted elemental abundances is provided in Table 1. This approach allows us to focus specifically on the chemical evolution while maintaining consistent physical conditions throughout the simulation.

The low temperatures in the core's inner region indicate an early stage of star formation, suggesting the chemical timescale is likely to be of the order of several tens of thousands of years. Previous modeling of self-consistent collapse demonstrates that during these initial phases, both the physical structure and chemical evolution undergo minimal changes, with any significant alterations confined to the innermost region where collapse is actively occurring (Aikawa et al. 2021, Li et al. 2002). Since no additional observations of the water transitions have been made after the experiment by Caselli et al. (2012), in the following section we compare the results of our chemical model with their simulated spatial distribution of the water abundances on the dust grains and in the gas phase.

4 Results

The results of the modeling are presented in Figs 1 and 2. Figure 1 shows an overproduction (relative abundance $x(H_2O) > 10^{-8}$) of the gas-phase water in the innermost cold and dense region by the two-phase model. Instead, the value of $x(H_2O) = 6 \times 10^{-10}$ realized in the three-phase model agrees with the results by Caselli et al. (2012). The presence of the surface and the bulk ice phases in our chemical model leads to a decrease in the water available for subsequent desorption to the gas phase. When the surface abundance of a species increases, some its fraction undergoes transfer to the bulk phase. This transfer rate is directly proportional to the surface abundance of the molecule in question: higher surface concentrations result in greater bulk deposition rates. Under conditions of low temperature and high density, water formation dominates over destruction processes, leading to efficient bulk ice storage. Notably, desorption can only occur from surface layers, not from the bulk. At the specified conditions of gas density (8×10^6 cm^{-3}) and dust temperature (6 K), water primarily forms on dust grain surfaces. Therefore, the substantial production

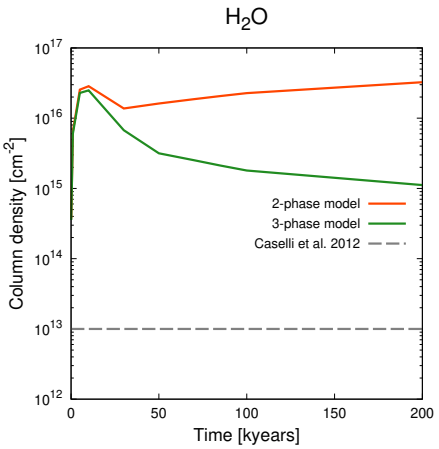


Figure 2 Modeled gas-phase water column densities for both two-phase and three-phase chemical regimes compared with the observational lower limit established by Caselli et al. (2012).

of surface water leads to significant bulk ice deposition. Our model considers a fixed surface reservoir of 5 monolayers, while allowing for unlimited bulk accumulation – typically reaching several hundred monolayers under these conditions. Bulk formation initiates even when surface monolayers are not completely filled, though the effect remains negligible in such cases. The bulk sequestration mechanism results in a substantial reduction of water vapor abundance, despite the nearly constant total water content on dust grains. The key factor is the water fraction available on the grain surface rather than the total ice inventory.

Analysis of the reaction rates shows that gas-phase water primarily originates from grain-surface chemistry. This result is in agreement with early findings. The dominant formation pathway occurs through the surface reaction s-H + s-OH $\longrightarrow$ s-H_2O. Immediately after formation, the majority ($\sim$95%) of water molecules undergo rapid sequestration into the bulk ice phase. The remaining fraction is subject to reactive desorption. This mechanism serves as the primary channel for replenishing gas-phase water in cold, dense environments, maintaining the observed balance between ice mantle growth and molecular gas abundances.

Moving outward from the core center, the environment becomes progressively less dense and slightly warmer, resulting in reduced bulk deposition rates and greater water retention on grain surfaces. In the outermost, most diffuse regions, bulk ice formation effectively ceases to occur, resulting in convergence of water abundance profiles between the 2-phase and 3-phase models.

5 Discussion and Conclusions

A specific feature of the 3-phase model is a significantly lower gas-phase water column density than in the 2-phase model, with the difference exceeding an order of magnitude at later times. This is related to the fact that in the 3-phase model water molecules are efficiently buried in thick icy mantles and are unavailable for desorption mechanisms. This specific distribution of water molecules is further illustrated in Fig. 1. In the 2-phase model, solid water abundance stays nearly constant everywhere in the core, except for its illuminated outer envelope. It is interesting that while in the 3-phase model water content in the bulk is nearly the same as its total surface content in the 2-phase model, 3d-bulk and 3d-surface water abundances do not sum up to its 2d-surface abundance. So, apparently the role of the layered mantle is not limited to just hiding some water from external processes, and there is some additional water (or rather oxygen) sink in the 3-phase model, which is not operative in the 2-phase model. This deserves further investigation.

As we mentioned earlier, in the core envelope the 2-phase and 3-phase models do not differ, reflecting the fact that in the outer core region desorption prevents the bulk from forming. Note, however, that even in this case water is mostly confined to solid phase.

Overall, we conclude that accounting for the layered mantle structure is vital for reproducing water evolution in cold dark environments. This structure does not simply divide water between two layers. Apparently, the presence of a chemically reactive surface and a more inert bulk launches or quenches some chemical pathways,

which are not drastically important for water production, but may be more important for other molecules. This problem deserves more thorough study.

References

Aikawa et al. (2021) ApJ 552, 639.
Borshcheva E.V., Wiebe D.S. (2022) Astron. Rep. 66, 393.
Caselli P., Keto E., Bergin E.A. et al. (2012) ApJL 759, L37.
Galli P.A.B., Loinard L., Bouy H. et al. (2012) A&A 630, A137.
Cheung A.C., Rank D.M., Townes C.H. et al. (1969) Nature 221, 626.
Hasegawa T.I., Herbst E. (1993) MNRAS 263, 589.
Izidoro A., Piani L. (2022) Elements 18, 181.
Kirsanova M.S., Baklanov P.V., Vasiliev E.O. et al. (2025) Physics Uspekhi 68, 278 293.
Kochina O.V., Wiebe D.S., Kalenskii S.V., Vasyunin A.I. (2013) Astron. Rep. 57, 818.
Kochina O.V., Wiebe D.S., Pavluychenkov Ya.N. et al., in prep.
Lee H.-H., Bettens R.P.A., Herbst E. (1996) A&A 119, 111.
Li et al. (2002) ApJ 792, 812.
Maitrey S., Majumdar L., Manilal V. et al. (2025) A&A 699, A332.
Ruaud M., Gorti U. (2019) ApJ 885, 146.
Semenov D., Wiebe D. (2011) ApJS 196, 25.
Snyder L. E., Buhl D. (1969) ApJ 155, L65.
van Dishoeck E.F., Kristensen L.E., Mottram J.C. et al. (2021) A&A 648, A24.
Wiebe D.S., Molyarova T.S., Akimkin V.V. et al. (2019) MNRAS 485, 1843.